All-Silicon Waveguide Avalanche Photodetectors With Ultrahigh Gain-Bandwidth Product and Low Breakdown Voltage

Haike Zhu, Linjie Zhou, *Member, IEEE*, Yanyang Zhou, Qianqian Wu, Xinwan Li, *Senior Member, IEEE*, and Jianping Chen

***Abstract*—We investigate the avalanche effect in 250 μm long silicon waveguides integrated with periodically interleaved p-n junctions. The surface state absorption is enhanced by reducing the waveguide width. Upon a bias voltage of -5.9 V, the measured responsivity is 2.33 A/W with a dark current of 0.78 μA. The avalanche gain is 284 and the 3-dB bandwidth is 3.6 GHz, leading to an ultrahigh gain-bandwidth product of 1.02 THz. The avalanche photocurrent is stable with time below -6 V when $\sim$1 mW on-chip optical power is launched. The photodetector has a linear response to optical power and can be readily integrated with other silicon photonic devices.**

***Index Terms*—Avalanche photodetector (APD), high-speed integrated optoelectronics, photodiodes, surface state absorption (SSA), silicon photonics.**

I. Introduction

Silicon waveguide has been proved to be an ideal platform for light transmission not only for its compact size, but also for its low loss in telecommunication wavelengths [1]–[3]. Because of its large indirect bandgap of 1.12 eV, silicon is not the optimal material for photodetection in the near-infrared wavelength range. However, all-silicon photodetection is still possible by utilizing several mechanisms, such as middle-bandgap absorption (MBA), two photon absorption (TPA), and surface state absorption (SSA) etc. The MBA has high responsivity [4]–[7], but extra ion implantation and well-controlled annealing processes are needed. TPA is a nonlinear effect which requires high optical power to generate detectable photocurrent. Usually resonance structures are employed to improve the responsivity [8]–[11], whilst the detection also becomes wavelength-dependent. SSA is another mechanism that has been applied in all-silicon photodetection [12], [13]. Such absorption is relatively weak and occurs on the surface of a waveguide. With a good optical mode field coverage on the surface [12], the responsivity of SSA can be improved.

Manuscript received January 31, 2014; revised April 23, 2014 and May 22, 2014; accepted May 27, 2014. This work was supported in part by the 973 program (ID2011CB301700), the 863 program (2013AA014402), the National Natural Science Foundation of China (61127016, 61107041), and the Science and Technology Commission of Shanghai Municipality Project (12XD1406400).

The authors are with the State Key Laboratory of Advanced Optical Communication Systems and Networks, Department of Electronic Engineering, Shanghai Jiao Tong University, Shanghai 200240, China (e-mail: wtxyxxl@sjtu.edu.cn; ljzhou@sjtu.edu.cn; zhouyanyang88@sjtu.edu.cn; wuqianqian91@sjtu.edu.cn; lixinwan@sjtu.edu.cn; jpchen62@sjtu.edu.cn).

Color version of one or more of the figures in this paper are available online at http://ieeexplore.ieee.org.

Digital Object Identifier 10.1109/JSTQE.2014.2328233

Even though the responsivity of all-silicon photodetection can be improved by optimizing the waveguide and device structures, it is still two to four magnitudes lower than that of III–V or Ge photodetectors, making them inefficient and cannot be used in the receiver end. However we can amplify the photocurrent by using the avalanche gain process. Silicon is widely used as avalanche photodetectors (APDs) working in wavelengths below 1.3 μm [14]–[17], and is also used as an avalanche layer for Ge–Si APDs working in telecommunication wavelengths [18]–[20]. Benefiting from the low hole-to-electron ionization ratio k of silicon, these devices possess high gain-bandwidth-product (GBP) and low multiplication noise. Recently, all-silicon APDs working in telecommunication wavelengths have been reported based on the MBA mechanism [21], [22]. High responsivity and high speed were achieved, suitable for on-chip photodetection. However, the breakdown voltage is very high due to the p-i-n junction [21]. In Ref. [22], as a microring is used to excite the TPA effect, its detection is wavelength dependent.

In our previous work [23], we reported a silicon waveguide integrated with periodically interleaved p-n junctions used as an on-chip optical power monitor. Due to the good electric field coverage on the waveguide surface especially on the waveguide sidewalls, the SSA effect is enhanced and more current is collected in this device than in p-i-n or lateral p-n structures. In this paper, we will study the avalanche effect in such a waveguide with an improved design. First, we increase the doping concentration to lower the breakdown voltage, which reduces the power consumption when the detector is working in the avalanche mode. Second, we shorten the device length to reduce the device footprint and improve the 3-dB bandwidth. Third, we narrow the waveguide to make more optical mode field residing on the waveguide surface. Measurements show that our device can achieve a high GBP under a low breakdown voltage. Meanwhile a high responsivity of over 2 A/W is achieved while the dark current is still below 1 μA. Under a proper working voltage, the avalanche photodetector is stable with time.

II. Device Structure and Fabrication

Fig. 1(a) shows the microscope images of three waveguide photodetectors. The waveguide active section length is 250 μm and the widths are 500, 400, and 300 nm. Fig. 1(b) shows the schematic of the silicon waveguide integrated with periodically interleaved p-n junctions. The waveguide height is 220 nm and the slab height is 60 nm. Lightly doped p and n regions with

1077-260X © 2014 IEEE. Personal use is permitted, but republication/redistribution requires IEEE permission.
See http://www.ieee.org/publications_standards/publications/rights/index.html for more information.

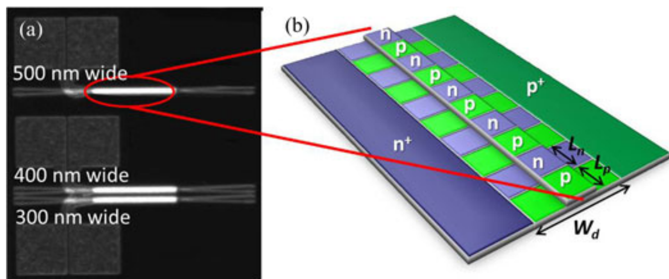

Fig. 1. (a) Microscope image of our devices. (b) Schematic of the silicon waveguide integrated with periodically interleaved p-n junctions.

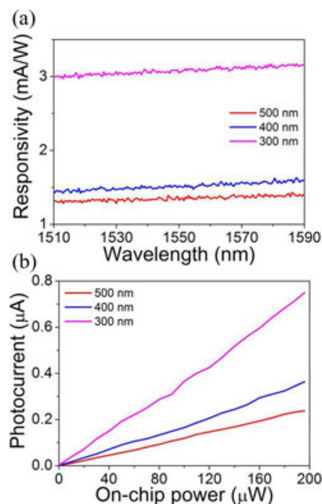

Fig. 2. (a) Measured responsivity as a function of wavelength for various waveguide widths. (b) Measured photocurrent as a function of on-chip power. The bias voltage is set at −1 V.

dimensions of $W_d = 1.5\ \mu\text{m}$, $L_p = 0.7\ \mu\text{m}$, and $L_n = 0.6\ \mu\text{m}$ are periodically patterned along the silicon waveguide. Beside the p/n doping region is the heavily doped p^+/n^+ region for ohmic contact with metal wires.

The devices were fabricated using the IME standard complementary metal–oxide–semiconductor (CMOS) process [24]. The p-type doping (Boron) was first implanted to cover the entire waveguide and then n-type doping (Phosphorus, higher dose) was introduced to compensate the original doping to form the interleaved p-n junctions. The resultant doping concentration for p regions is $\sim 4 \times 10^{17}\ \text{cm}^{-3}$, and for n regions is $\sim 1 \times 10^{18}\ \text{cm}^{-3}$. The compensation doping makes it easy to form interleaved junctions [25]. The heavily doped p^+/n^+ (Boron/Phosphorus) region has a doping concentration of $\sim 10^{20}\ \text{cm}^{-3}$. Rapid thermal annealing at 1030 °C for 5 s was used after ion implantation. This temperature can anneal out most of the ion implantation-induced defects including di-vacancies [26] and also interstitial clusters [27], which are the main defects responsible for MBA effect [4].

III. Experiments

A. Low-Bias Response

Fig. 2(a) shows the measured responsivity of our devices. The input laser light is transverse-electrically polarized by using a polarization controller. The wavelength is scanned from 1510 to 1590 nm with a step of 0.2 nm, while the current is recorded by an I/V measure unit (Agilent B2912A) through a pair of metal probes connecting the device electrical pads. The devices are biased at −1 V, where the avalanche effect is relatively weak. The input power from the fiber is ∼0.2 mW. The insertion loss (fiber-to-fiber) is ∼16 dB, which is mainly caused by the coupling loss. Assuming the input and output coupling losses are equal, the estimated coupled optical power in the waveguide is 31.6 μW. We can see that the responsivity increases as the waveguide width decreases. The responsivity of the 300 nm wide waveguide is over two times higher than that of the other two wider waveguides.

Fig. 2(b) shows the measured photocurrent as a function of on-chip power at −1 V bias. The laser light at 1550 nm is amplified by an erbium-doped optical fiber amplifier (EDFA) to boost up the optical power, followed by a 0.8-nm bandwidth optical filter to suppress the amplified spontaneous emission noise. The input power is adjusted by tuning the EDFA gain. The photocurrent is obtained by subtracting the dark current from the measured current under illumination. The photocurrent increases linearly with on-chip power as the SSA effect is a linear process [28].

B. Avalanche Response

We next increase the reverse bias and the *I–V* curves of our devices are plotted in Fig. 3(a). The dark current rises with the reverse bias voltage. The avalanche effect becomes very strong at around −6.8 V, where the dark current increases very quickly. After −7.5 V, the increment of dark current slows down and reaches ∼80 mA at −10 V. When 31.6 μW on-chip optical power is applied, the measured currents under illumination in the 400 and 500 nm wide waveguides are close and see a rapid growth from −6 to −7 V. The current in the 300 nm wide waveguide is higher than the other two devices with 10.7 μA at −5.5 V and 1 mA at −6.2 V. It increases 100 times within the 0.7 V range. At around −7 V, the currents of all the three devices reach almost the same level. At around −9 V, the currents are dominated by the dark current. The slow increment after −7 V is mainly due to the space-charge-limited current [29].

Fig. 3(b) shows the photocurrent generated by the 300 nm wide waveguide as a function of on-chip power at various reverse biases. The photocurrent still keeps a well linear response to on-chip power under the avalanche effect. However, as the reverse bias increases, especially at −6 V and −6.1 V as shown in the inset of Fig. 3(b), the photocurrent becomes unstable. The avalanche process is statistical in nature because every electron–hole pair generated at a given distance in the depletion region is independent and does not experience the same multiplication [30]. The fluctuation of gain is caused by excess noise which is a function of hole-to-electron ionization ratio. As the electric field increases with the reverse bias, the hole-to-electron ionization ratio increases [31], leading to an increased excess noise. As a result the gain is more unstable at a high reverse bias.

Fig. 3(c) shows the extracted responsivity and avalanche gain of the 300 nm wide waveguide as a function of reverse bias. The responsivity is 1.45 mA/W at 0 V and rises with the reverse bias. An ultra-high responsivity of 528 A/W is achieved at −7 V. Although the dark current is relatively high (0.66 mA), it is still

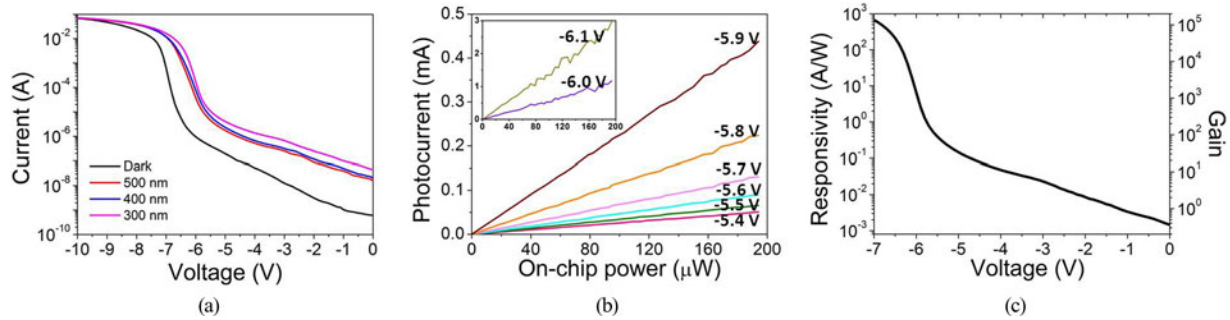

Fig. 3. (a) Measured current as a function of reverse bias for the three devices. (b) Photocurrent as a function of on-chip power at various high reverse biases for the 300 nm wide waveguide. Inset: photocurrent curves at −6 and −6.1 V. (c) Extracted responsivity and avalanche gain as a function of reverse bias for the 300 nm wide waveguide.

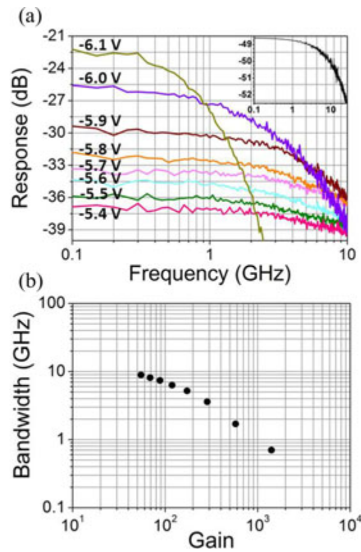

Fig. 4. (a) Measured frequency responses of the 300 nm wide waveguide at various reverse biases near the breakdown voltage. Inset: frequency response at −2.6 V. (b) 3-dB bandwidth changes as a function of avalanche gain.

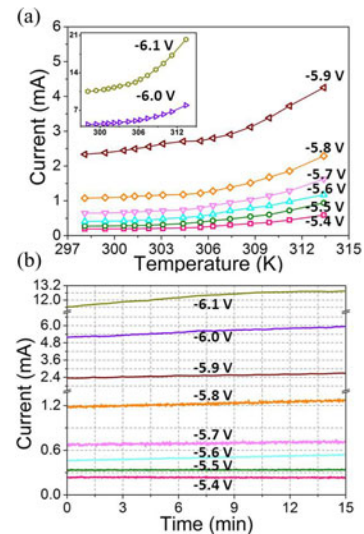

Fig. 5. (a) Temperature stability of current at various reverse biases. Inset: current variation at −6 and −6.1 V. (b) Temporal stability of current at various reverse biases.

more than 20 times smaller than the photocurrent. The avalanche gain is obtained by normalizing the responsivity with that at −1.2 V bias where the junction is nearly fully depleted and the avalanche effect is relatively weak. The gain rises up rapidly with the reverse bias, especially after −5.5 V. The gain is about 10^2 at −5.5 V, 10^3 at −6.1 V, 10^4 at −6.4 V, and 10^5 at −7 V, increasing by 10^3 times within the 1.5 V range.

C. Gain-Bandwidth Product

We next characterize the small-signal radio frequency (RF) response of our devices. A vector network analyzer (VNA, Agilent 8722D) is used as the RF signal source, followed by an RF amplifier to drive a modulator. The modulated optical signal is coupled into the device and the generated photocurrent is collected by a pair of 40 GHz microwave probes. The signal is then sent back to the VNA. The input wavelength is fixed at 1550 nm. The VNA scans from 100 MHz to 26.5 GHz. The frequency response of the device is normalized with a commercial 70 GHz photodetector. Fig. 4(a) shows the frequency response of the 300 nm wide waveguide at various reverse biases. The 3-dB bandwidth decreases from to 3.6 GHz when the reverse bias increases from −5.4 to −5.9 V. It further decreases to 0.6 GHz at −6.1 V.

Fig. 4(b) shows the 3-dB bandwidth as a function of avalanche gain. The 3-dB bandwidth decreases as avalanche gain increases. The GBP is ∼490 GHz at −5.4 V and increases to the maximum of ∼1.02 THz at −5.9 V where the responsivity is ∼2.33 A/W and the dark current is 0.64 μA, as seen from Fig. 3(c). It falls to ∼988 GHz at −6.1 V.

D. Temperature Stability

The dark current and avalanche gain are strong functions of temperature [32]. To characterize the temperature effect, we measure the current at various temperatures by placing a microheater (Thorlab TED 4015) under the chip. Fig. 5(a) shows the measured results when an on-chip power of ∼1 mW is applied. The current gradually increases with the rising temperature. The increment is more significant for larger reverse bias and higher temperature. For example, at −6.1 V the current at ∼314 K is over two times larger than that at ∼298 K as shown in the inset of Fig. 5(a).

Fig. 5(b) shows the current as a function of time at various reverse biases at room temperature ∼298 K. The measurement

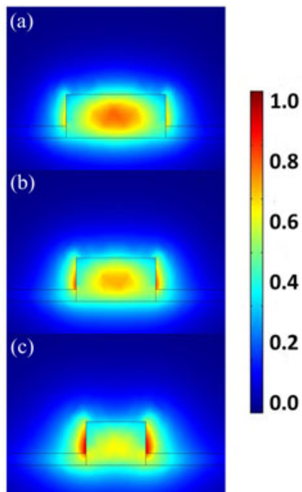

Fig. 6. Simulated optical mode electric field distributions in the waveguides with widths of (a) 500, (b) 400, and (c) 300 nm.

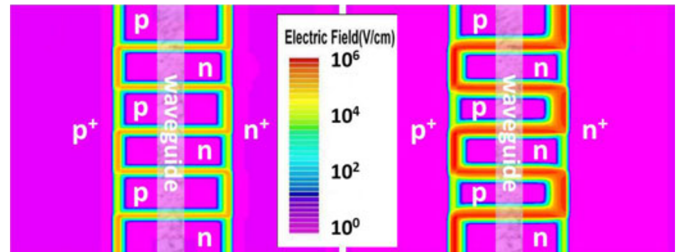

Fig. 7. Simulated junction electric field distributions in the 300 nm wide waveguide at (a) 0 and (b) −6 V biases.

is carried out in 15 min with a sampling interval of 1 s by using Agilent B2912A. The on-chip power is also ~1 mW. One can see that the current is relatively constant with time when the bias is small (below −6 V). At a higher reverse bias, the current increases with time more significantly.

IV. Analysis and Discussion

A. Optical Mode Field Distribution and Photon Absorption

The SSA effect is the main absorption mechanism in our silicon waveguides [23]. In order to enhance the absorption, waveguide dimensions need to be carefully designed so that the surface states reside at the peak intensity of the waveguide optical mode. Baehr-Jones *et al.* [12] measured a responsivity of 36 mA/W in a 100 nm high and 500 nm wide silicon waveguide integrated with a 1.5 mm long p-i-n junction. However, as most of the silicon photonics devices today are based on the 220 nm high waveguide, we consider keeping the waveguide height while narrowing the width to improve the responsivity.

Fig. 6(a)–(c) shows the optical mode field distributions of the 500, 400, and 300 nm wide waveguides, respectively. The results are obtained by mode analysis simulation from COMSOL. As waveguide width decreases, more optical mode field leaks from the waveguide to the cladding. The photon that can be absorbed is within 1 nm above the waveguide edge where surface states exist [33]. Under the same optical power, the average mode electric field on the 300 nm wide waveguide sidewall is 1.66 and 1.93 times higher than that of the 400 and 500 nm wide waveguides, respectively. The simulated propagation losses are 14.2, 13.6 and 11.8 dB/cm for the 500, 400 and 300 nm wide waveguides, respectively. As the waveguide is embedded with interleaved p-n junctions, the loss decreases as more optical field is located outside the silicon core.

To compare the responsivity of our 300 nm wide waveguide with Baehr-Jones' work [12], we choose the photocurrent measured at −1.2 V, where the junction is nearly fully depleted. The measured responsivity is 4.05 mA/W. Given the difference in waveguide length, the responsivity of our device is comparable to Baehr-Jones' work [12].

B. Electric Field Coverage and Current Gain

We use SILVACO to simulate the junction electric field distribution in the interleaved p-n junctions over three periods at 0 and −6 V as shown in Fig. 7(a) and (b), respectively. The peak electric field is 1.6×10^5 V/cm with a depletion width of 250 nm at 0 V, while it increases to 8.9×10^5 V/cm with a depletion width of 400 nm at −6 V. Under the peak electric field at −6 V, the electron and hole ionization rates are $1.22 \times 10^5\ \mathrm{cm}^{-1}$ and $6.13 \times 10^4\ \mathrm{cm}^{-1}$, respectively. The average hole-to-electron ionization ratio k in the depletion region is ~0.5 at −6 V, which allows our device to have a high avalanche gain with a low excess noise factor [34].

In Fig 7(b), we can see that even though the junctions are fully depleted, more than two-thirds of the waveguide is still without the coverage of electric field, which makes the detection not so efficient. This is mainly because of the relatively large doping window limited by the fabrication resolution. If a narrower doping window is chosen, the waveguide can be more fully covered by the electric field and the responsivity can hence be further improved.

C. Avalanche Buildup Time

In our previous work [23], we measured a 3-dB bandwidth of ~11.5 GHz with quite weak avalanche effect. In this work, we shortened the device length to 250 μm while keeping the same electrode design. A short electrode reduces the high-frequency transmission loss and the phase mismatch between the optical wave and the microwave. Therefore, the measured 3-dB bandwidth is improved to ~18.6 GHz at the low reverse bias of −2.6 V, as shown in the inset of Fig. 4(a).

However, as the avalanche gain rises up, the response time is mainly limited by the avalanche buildup time rather than by the travelling wave electrode [35]. Considering that the carrier drift velocity is saturated at such a high electric field when the avalanche effect occurs, Kuvas *et al.* gives the formula [36], $t = \tau M$, where t is the avalanche buildup time, τ is the intrinsic response time, and M is the avalanche gain. τ is experimentally obtained to be 0.5 ps by Kaneda [37]. In our experiment, the avalanche gain is 284 at −5.9 V, thus the avalanche buildup time is ~0.143 ns according to Kaneda's value of τ. It suggests the bandwidth of the 300 nm wide waveguide has an up limit of 6.99 GHz at −5.9 V.

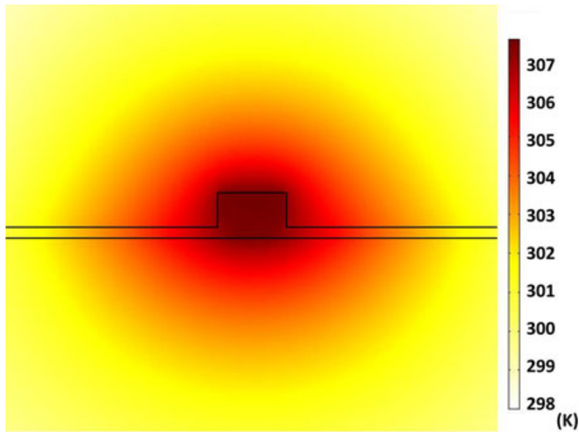

Fig. 8. Simulated temperature cross-sectional distribution in the 300 nm wide waveguide at -6.1 V.

D. Thermal Effect

When the avalanche effect occurs, the current through the p-n junctions increases quickly with reverse bias, giving rise to thermal heating in the device. As the waveguide cladding layer silicon dioxide is not a good thermal conductor, the heat generated will be mainly confined in the silicon layer, leading to raised temperature in the waveguide. We simulate the temperature distribution at -6.1 V in the 300 nm wide waveguide by using the heat transfer module from COMSOL, as shown in Fig. 8. Under the on-chip optical power of $\sim$1 mW, the power dissipation in the device is $11\ \mathrm{mA} \times 6.1\ V = 67.1$ mW extracted from the experimental result. Assuming heat is generated from the p-n junctions with a volume of $\sim 34.5\ \mu\mathrm{m}^3$, the power density of the heat source is $1.9\ \mathrm{mW}/\mu\mathrm{m}^3$. The ambient temperature is set to 298 K. Upon stationary analysis, we get a temperature rise of 9.5 K in the waveguide. If the reverse bias is reduced to -5.4 V, then the temperature rise is only 0.2 K. The raised temperature in the waveguide increases the current, which in turn generates more heat and further increases the temperature. A positive feedback forms, making the current gradually rise with time, which is more significant at -6.1 V but negligible at -5.4 V [see Fig. 5(b)].

V. Conclusion

We designed and fabricated all-silicon APDs using 250 μm long straight silicon waveguides integrated with periodically interleaved p-n junctions. The fabrication process is CMOS compatible and can be readily integrated with other silicon photonic devices. The photodetector is based on the SSA effect and is wavelength insensitive. More photocurrent is generated by the SSA effect by narrowing the silicon waveguide. The avalanche mode working regime is around the range of -5.5 to -7 V. Towards the high bias end, the device exhibits large responsivity and gain but at the price of instability, low bandwidth, and high power consumption. For example, the responsivity can be up to 528 A/W with a gain of 10^5 but the dark current is also as high as 0.66 mA. The scenario is quite the opposite towards the low bias end. Therefore, the working voltage needs to be set according to practical applications. A compromised value can be set as -5.9 V where a balanced performance can be achieved. With this bias, the responsivity is 2.33 A/W with a dark current of 0.78 μA. The GBP is 1.02 THz, which is the highest value achieved in silicon waveguide photodetectors so far. The voltage sensitivity of gain (dG/dV) is $2423\ \mathrm{V}^{-1}$ at -5.9 V. The high gain is benefited from the high doping concentration and the low ionization ratio.

Our device can also work as a power monitor if we decrease the working voltage off the avalanche regime. The responsivity is still over 1 mA/W at -1 V bias with a high bandwidth. The power consumption of the monitor is much lower compared to our previous work [23].

Acknowledgment

The authors acknowledge IME Singapore for device fabrication.

References

[1] B. Jalali and S. Fathpour, “Silicon photonics,” *J. Lightw. Technol.*, vol. 24, no. 12, pp. 4600–4615, Dec. 2006.
[2] N. Izhaky, M. T. Morse, S. Koehl, O. Cohen, D. Rubin, A. Barkai, G. Sarid, R. Cohen, and M. J. Paniccia, “Development of CMOS-compatible integrated silicon photonics devices,” *IEEE J. Sel. Topics Quantum Electron.*, vol. 12, no. 6, pp. 1688–1698, Nov. 2006.
[3] R. Pafchek, R. Tummidi, J. Li, M. A. Webster, E. Chen, and T. L. Koch, “Low-loss silicon-on-insulator shallow-ridge TE and TM waveguides formed using thermal oxidation,” *Appl. Opt.*, vol. 48, pp. 958–963, Feb. 2009.
[4] M. W. Geis, S. J. Spector, M. E. Grein, J. U. Yoon, D. M. Lennon, and T. M. Lyszczarz, “Silicon waveguide infrared photodiodes with >35 GHz bandwidth and phototransistors with 50 AW^{-1} response,” *Opt. Exp.*, vol. 17, pp. 5193–5204, Mar. 2009.
[5] D. F. Logan, P. E. Jessop, and A. P. Knights, “Modeling defect enhanced detection at 1550 nm in integrated silicon waveguide photodetectors,” *J. Lightw. Technol.*, vol. 27, no. 7, pp. 930–937, Apr. 2009.
[6] D. F. Logan, P. Velha, M. Sorel, R. M. De La Rue, A. P. Knights, and P. E. Jessop, “Defect-enhanced silicon-on-insulator waveguide resonant photodetector with high sensitivity at 1.55 μm,” *IEEE Photon. Technol. Lett.*, vol. 22, no. 20, pp. 1530–1532, Oct. 2010.
[7] H. Yu, D. Korn, M. Pantouvaki, J. Van Campenhout, K. Komorowska, P. Verheyen, G. Lepage, P. Absil, D. Hillerkuss, L. Alloatti, J. Leuthold, R. Baets, and W. Bogaerts, “Using carrier-depletion silicon modulators for optical power monitoring,” *Opt. Lett.*, vol. 37, pp. 4681–4683, Nov.2012.
[8] T. Tanabe, H. Sumikura, H. Taniyama, A. Shinya, and M. Notomi, “All-silicon sub-Gb/s telecom detector with low dark current and high quantum efficiency on chip,” *Appl. Phys. Lett.*, vol. 96, pp. 101103–1–101103-3, Feb. 2010.
[9] H. Chen and A. W. Poon, “Two-photon absorption photocurrent in p-i-n diode embedded silicon microdisk resonators,” *Appl. Phys. Lett.*, vol. 96, pp. 191106–1–191106-3, May 2010.
[10] T. K. Liang, H. K. Tsang, I. E. Day, J. Drake, A. P. Knights, and M. Asghari, “Silicon waveguide two-photon absorption detector at 1.5 μm wavelength for autocorrelation measurements,” *Appl. Phys. Lett.*, vol. 81, pp. 1323–1325, Aug. 2002.
[11] H. Zhu, L. Zhou, X. Sun, J. Xie, X. Li, and J. Chen, “Photocurrent generation in a microdisk resonator integrated with interleaved P-N junctions,” presented at the Conf. Lasers Electro-Opt., San Jose, CA, USA, 2013, Paper JTh2A.38.
[12] T. Baehr-Jones, M. Hochberg, and A. Scherer, “Photodetection in silicon beyond the band edge with surface states,” *Opt. Exp.*, vol. 16, pp. 1659–1668, Jan. 2008.
[13] H. Chen, X. Luo, and A. W. Poon, “Cavity-enhanced photocurrent generation by 1.55μm wavelengths linear absorption in a p-i-n diode embedded silicon microring resonator,” *Appl. Phys. Lett.*, vol. 95, pp. 171111-1–171111-3, Oct. 2009.
[14] M. Ghioni, A. Lacaita, G. Ripamonti, and S. Cova, “All-silicon avalanche photodiode sensitive at 1.3 μm with picosecond time resolution,” *IEEE J. Quantum Electron.*, vol. 28, no. 12, pp. 2678–2681, Dec. 1992.

[15] A. Rochas, A. R. Pauchard, P. A. Besse, D. Pantic, Z. Prijic, and R. S. Popovic, "Low-noise silicon avalanche photodiodes fabricated in conventional CMOS technologies," *IEEE Trans. Electron Dev.*, vol. 49, no. 3, pp. 387–394, Mar. 2002.
[16] H.-S. Kang, M.-J. Lee, and W.-Y. Choi, "Si avalanche photodetectors fabricated in standard complementary metal-oxide-semiconductor process," *Appl. Phys. Lett.*, vol. 90, pp. 151118-1–151118-3, Apr. 2007.
[17] K. Iiyama, H. Takamatsu, and T. Maruyama, "Hole-injection-type and electron-injection-type silicon avalanche photodiodes fabricated by standard 0.18-μm CMOS process," *IEEE Photon. Technol. Lett.*, vol. 22, no. 12, pp. 932–934, Jun. 2010.
[18] S. Assefa, F. Xia, and Y. A. Vlasov, "Reinventing germanium avalanche photodetector for nanophotonic on-chip optical interconnects," *Nature*, vol. 464, pp. 80–84, Mar. 2010.
[19] N. Duan, T. Y. Liow, A. E. Lim, L. Ding, and G. Q. Lo, "310 GHz gain-bandwidth product Ge/Si avalanche photodetector for 1550 nm light detection," *Opt. Exp.*, vol. 20, pp. 11031–11036, Apr. 2012.
[20] W. S. Zaoui, H.-W. Chen, J. E. Bowers, Y. Kang, M. Morse, M. J. Paniccia, A. Pauchard, and J. C. Campbell, "Frequency response and bandwidth enhancement in Ge/Si avalanche photodiodes with over 840GHz gain-bandwidth-product," *Opt. Exp.*, vol. 17, pp. 12641–12649, Jul. 2009.
[21] J. J. Ackert, A. S. Karar, D. J. Paez, P. E. Jessop, J. C. Cartledge, and A. P. Knights, "10 Gbps silicon waveguide-integrated infrared avalanche photodiode," *Opt. Exp.*, vol. 21, pp. 19530–19537, Aug. 2013.
[22] Y. Li, S. Feng, Y. Zhang, and A. W. Poon, "Sub-bandgap linear-absorption-based photodetectors in avalanche mode in PN-diode-integrated silicon microring resonators," *Opt. Lett.*, vol. 38, pp. 5200–5203, Dec. 2013.
[23] H. Zhu, L. Zhou, X. Sun, Y. Zhou, X. Li, and J. Chen, "On-chip optical power monitor using periodically interleaved P-N junctions integrated on a silicon waveguide," *IEEE J. Sel. Topics Quantum Electron.*, vol. 20, no. 4, pp. 1–8, Jan. 2014.
[24] K.-W. Ang, Q. Fang, J.-F. Song, Y.-Z. Xiong, M.-B. Yu, G.-Q. Lo, and D.-L. Kwong, "Silicon modulators and germanium photodetectors on SOI: Monolithic integration, compatibility, and performance optimization," *IEEE J. Sel. Topics Quantum Electron.*, vol. 16, no. 1, pp. 307–315, Jan. 2010.
[25] X. Xiao, H. Xu, X. Li, Y. Hu, K. Xiong, Z. Li, T. Chu, Y. Yu, and J. Yu, "25 Gbit/s silicon microring modulator based on misalignment-tolerant interleaved PN junctions," *Opt. Exp.*, vol. 20, pp. 2507–2515, Jan./Feb. 2012.
[26] M. W. Geis, S. J. Spector, M. E. Grein, R. T. Schulein, J. U. Yoon, D. M. Lennon, S. Deneault, F. Gan, F. X. Kaertner, and T. M. Lyszczarz, "CMOS-compatible all-Si high-speed waveguide photodiodes with high responsivity in near-infrared communication band," *IEEE Photon. Technol. Lett.*, vol. 19, no. 3, pp. 152–154, Feb. 2007.
[27] S. Libertino, S. Coffa, and J. Benton, "Formation, evolution, and annihilation of interstitial clusters in ion-implanted Si," *Phys. Rev. B*, vol. 63, pp.195206–1–195206-14, Apr. 2001.
[28] N. Johnson, W. Jackson, and M. Moyer, "Optical spectroscopy of the trivalent silicon defect at the Si-SiO_2 interface," *Phys. Rev. B*, vol. 31, pp. 1194–1197, Jan. 1985.
[29] S. M. Sze and K. K. Ng, "Physics and properties of semiconductors," in *Physics of Semiconductor Devices*, 3rd ed. Hoboken, NJ, USA: Wiley, 2007, ch. 1.5.8, pp. 663–664.
[30] S. M. Sze and K. K. Ng, "Photodetectors and solar cells," in *Physics of Semiconductor Devices*, 3rd ed. Hoboken, NJ, USA: Wiley, 2007, ch. 13.4.2, p. 685.
[31] S. M. Sze and K. K. Ng, "Photodetectors and solar cells," in *Physics of Semiconductor Devices*, 3rd ed. Hoboken, NJ, USA: Wiley, 2007, ch. 13.4.4, pp. 689–694
[32] C. R. Crowell, "Temperature dependence of avalanche multiplication in semiconductors," *Appl. Phys. Lett.*, vol. 9, pp. 242–244, Aug. 1966.
[33] V. Heine, "Theory of surface states," *Phys. Rev.*, vol. 138, pp. A1689–A1696, Jun. 1965.
[34] R. D. Baertsch, "Noise and ionization rate measurements in silicon photodiodes," *IEEE Trans. Electron Dev.*, vol. 13, no. 12, pp. 987–987, Dec. 1966.
[35] C. A. Lee, "Time dependence of avalanche processes in silicon," *J. Appl. Phys.*, vol. 38, pp. 2787–2796, Dec. 1967.
[36] R. Kuvas and C. A. Lee, "Quasistatic approximation for semiconductor avalanches," *J. Appl. Phys.*, vol. 41, pp. 1743–1755, Dec. 1970.
[37] T. Kaneda and H. Takanashi, "Avalanche buildup time of silicon avalanche photodiodes," *Appl. Phys. Lett.*, vol. 26, pp. 642–644, Jun. 1975.

Haike Zhu received the B.S. degree from the Physics Department, Sichuan University, Chengdu, China, in 2010. He is currently working toward the Ph.D. degree at the State Key Laboratory of Advanced Optical Communication Systems and Networks, Department of Electronic Engineering, Shanghai Jiao Tong University, Shanghai, China. His research interests include high-speed integrated silicon photodetectors, and modulators.

Linjie Zhou (M'04) received the B.S. degree in microelectronics from Peking University, Beijing, China, in 2003, and the Ph.D. degree in electronic and computer engineering from the Hong Kong University of Science and Technology, Clear Water Bay, Hong Kong, in 2007. From 2007 to 2009, he was a Postdoctoral Researcher at the University of California, Davis. He is currently an Associate Professor at the State Key Laboratory of Advanced Optical Communication Systems and Networks, Shanghai Jiao Tong University, Shanghai, China.

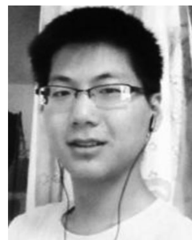

Yanyang Zhou received the B.S. degree in electrical engineering from PLA Information Engineering University, Zhengzhou, China, in 2011. He is currently a graduate student with the State Key Laboratory of Advanced Optical Communication Systems and Networks, Department of Electronic Engineering, Shanghai Jiao Tong University, Shanghai, China. His research interests include silicon modulators, microwave low-noise amplifiers, and High-speed circuits.

Qianqian Wu received the B.S. degree in electrical engineering from Anhui University, Hefei, China, in 2012. She is currently a graduate student with the State Key Laboratory of Advanced Optical Communication Systems and Networks, Department of Electronic Engineering, Shanghai Jiao Tong University, Shanghai, China. Her current research interests include nonlinear optics and silicon thermo-optic devices.

Xinwan Li (SM'01) received the M.S. degree from Shanghai University, Shanghai, China, in 1993, and the Ph.D. degree from Shanghai Jiao Tong University, Shanghai, in 2005. Since 1993, he has been with Shanghai Jiao Tong University, where he is currently a Professor. From 1997 to 1998, he was with Essex University, Colchester, U.K., as a Research Assistant. In 2001, he joined OPCOM Inc. as an Engineer and as a Visiting Professor of Chonbuk National University in 2007. His main research interests include optical switching technologies and advanced optical fiber components. He is a Senior Member of the IEEE Photonics Society and the Chair of the IEEE Communications Society Shanghai Chapter.

Jianping Chen received the B.S. degree from Zhejiang University, Hangzhou, China, in 1983, and the M.S. and Ph.D. degrees from Shanghai Jiao Tong University, Shanghai, China, in 1986 and 1992, respectively. He is currently a Professor with the State Key Laboratory of Advanced Optical Communication Systems and Networks, Department of Electronic Engineering, Shanghai Jiao Tong University. His main research interests include photonic devices and signal processing, optical networking, and sensing optics. He is also a Principal Scientist of 973 project in China.